Real-time wide dynamic range spectrometer using a rapidly wavelength-switchable terahertz parametric source

SOTA MINE,[1,*] KODO KAWASE,[1] AND KOSUKE MURATE[1]

[1]*Department of Electronics, Nagoya University, Furocho, Nagoya, 464-8603, Japan*
**Corresponding author: mine.sota@b.mbox.nagoya-u.ac.jp*

Received XX Month XXXX; revised XX Month, XXXX; accepted XX Month XXXX; posted XX Month XXXX (Doc. ID XXXXX); published XX Month XXXX

In this study, we demonstrate real-time terahertz (THz) spectroscopy using a rapidly wavelength-switchable injection-seeded THz parametric generator. We developed a wavelength-switchable external cavity diode laser using a digital micromirror device as a seed source for the generator. We realized fast acquisition of THz spectra by switching the wavelength of the laser for each pump beam pulse. This system can rapidly switch wavelength and easily increase the number of measurement wavelengths, and also has a wide dynamic range, of more than 75 dB, and high stability. Furthermore, by combining this system with THz parametric detection, all wavelengths can be detected in a single frame using a near infrared camera for real-time reagent measurement.

There have been many studies about real-time terahertz (THz) measurements in recent years [1–11]. With THz time domain spectroscopy, rapid measurement is possible; however, it is not suitable for penetrating shields with high scattering, such as mail envelopes, and the dynamic range is reduced above the 1 THz region, where the fingerprint spectra of many reagents lie [1–6]. Studies on real-time spectroscopy have also been conducted using wavelength-tunable THz-wave sources pumped by high repetition-rate lasers [7,8] or by using multi-wavelength THz-wave sources [11–13]. However, there has been no report on a practical, real-time system that satisfies the requirements with respect to dynamic range and the number of measurement wavelengths.

Injection-seeded THz-wave parametric generators (is-TPGs) have a high peak power output (~100 kW) and wide tunability (wavelength of 60–750 μm, frequency of 0.4–5 THz) [13–15]. It is also possible to detect THz-waves with high sensitivity by up-converting THz-waves to near-infrared (NIR) beams in the reverse process of an is-TPG and observing them using a NIR camera. Such a spectrometer combines parametric generation and detection and shows a wide dynamic range, of up to 125 dB [16]. Our is-TPG spectrometer is barely affected by scattering or refraction, and is able to penetrate through shields because it measures in the frequency domain and the detection area is large (a few millimeters). Therefore, we expect that real-time measurement using this is-TPG spectrometer will find many applications, including the inspection of drugs through thick shields [17]. Against this background, we developed a multi-wavelength is-TPG, which can generate multiple THz wavelengths simultaneously [11–13]. However, multi-wavelength is-TPGs have certain problems, such as parametric gain competition among the THz wavelengths and the need to match the number of external cavity diode lasers (ECDLs) for injection seeding with the number of THz wavelengths.

Thus, we aimed to develop a real-time THz spectroscopic system by rapidly switching the wavelength of the is-TPG. An is-TPG generates THz waves by inputting pump and seed beams to a $MgO:LiNbO_3$ crystal; the output wavelength is tuned by changing the wavelength and injection angle of the seed beam to satisfy the noncollinear phase-matching condition [13]. In conventional is-TPG, we previously used a commercially available ECDL as a seed source, but this could not change the THz wavelength rapidly; its tuning speed was slow, at almost 1 THz/min. Therefore, we developed an ECDL with a rapidly switchable wavelength by introducing a digital micromirror device (DMD) as a wavelength selection mechanism [18,19]. A DMD is a micro-electrical-mechanical device in which micromirrors are arranged in an array, wherein each mirror can be independently controlled. Although there have been some reports of ECDLs with DMDs [20–22], our ECDL shows a higher signal-to-noise ratio, of >75 dB, and a higher output power, of nearly 300 mW, making it an ideal seed source for is-TPG [23].

Figure 1 shows the experimental setup of a rapidly tunable is-TPG that uses our developed ECDL (lower left part of the figure). We used a ring cavity as the resonator to suppress spatial hole burning and achieve stable oscillations. Furthermore, amplified spontaneous emission (ASE)-free, high signal-to-noise ratio output was made possible by the ring cavity because there was no ASE from the laser diode (OE-1040TA; Spectra Quest Lab, Inc., Japan); only a wavelength-selected beam can be output from the apparatus. In general, an ECDL selects a wavelength based on the angle of a mirror or diffraction grating; we used a DMD for this purpose in our system. The ASE from a laser diode was diffracted by the grating and focused onto the DMD. As shown in the upper left part of Fig. 1, when diffracted light is input to the DMD, the oscillation wavelength can be selected by tilting the micromirrors positioned according to the desired wavelength. The wavelength-selected beam was reflected slightly downward, into the plane of the diagram, and reflected by a D-shaped mirror to a different direction than that of the incident beam. The beam diameter was reduced by a pair of lenses for injection into the isolator, and for efficient coupling to the laser diode. By using a polarization beam splitter as the output mirror, the feedback rate was variable, so that the optimum laser power could be obtained.

The pump beam from the microchip laser and seed beam from the ECDL were input to the $LiNbO_3$ crystal to generate a THz-wave (Linewidth < 4 GHz); 11 mJ of the pump beam was injected into the $LiNbO_3$ crystal for generation and 3 mJ was used for detection. The seed beam was amplified to 300 mW and injected into the generation crystal. The achromatic optical setup, consisting of a diffraction grating and a lens pair in the seed beam path, ensures that the injection angle of the seed beam changes at each wavelength to automatically satisfy the phase-matching condition. The generated THz-wave was then input to the $LiNbO_3$ crystal after passing through the sample. During the detection process, the THz-wave was up-converted to a NIR beam (we call this the "detection Stokes beam"), which was detected by a NIR camera (GS3-U3-41C6NIR-C; Point Grey Research Inc., Canada) synchronized with the μ-chip laser. Each wavelength can be detected separately, given that the generation angle of each detection Stokes beam varies according to the wavelength due to the noncollinear phase-matching condition. Information for all wavelengths can be obtained in one shot by adjusting the exposure time of the NIR camera according to the number of wavelengths. Therefore, the frame rate and number of wavelengths are inversely proportional to each other. For example, when the repetition rate of the pump beam is 50 Hz, measurement of five wavelengths is possible at a frame rate of 10 Hz, while measurement of 10 wavelengths is possible at a frame rate of 5 Hz.

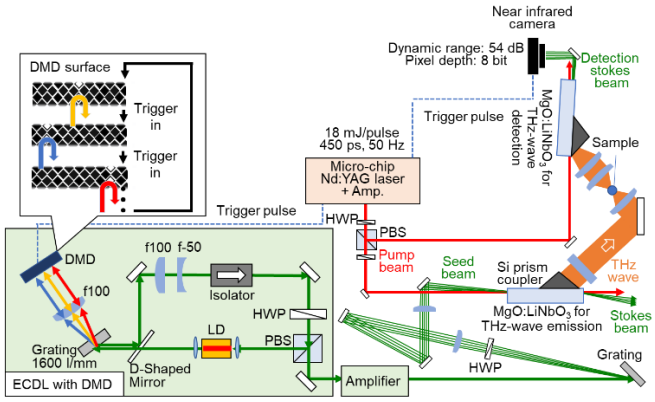

Fig. 1. Experimental setup of a rapidly wavelength-switchable injection-seeded THz parametric generator using an external cavity diode laser (ECDL) with a digital micromirror device (DMD).

Before using it for THz-wave generation, we analyzed some properties of our developed ECDL. Figure 2(a) shows the wavelength dependence of the output power. The wavelength tunable range was approximately 24 nm, (1,065–1,089 nm) and had a flat output from 1,065 nm to approximately 1,082 nm. The energy corresponding to wavelengths above 1,082 nm rapidly decreased due to the bandwidth of the LD (980–1,085 nm). The upper axis shows the corresponding frequency (in THz) when the ECDL was used as a seed source for the is-TPG. We confirmed that the ECDL could cover the 0.4–5 THz range, wherein we report is-TPG generation. Next, we measured the wavelength resolution of the ECDL, which was determined based on the focal length of the focusing lens to the DMD, the grating constant, and the size of the DMD's micromirrors. In our setup, the resolution was 0.04 nm. The is-TPG generated THz-waves correspond to the difference in frequency between the pump and seed beams. Therefore, the wavelength resolution of the ECDL determined the frequency resolution of the generated THz-wave, which in this case was approximately 10 GHz. Since the absorption linewidths of many reagents exceed 100 GHz, 10 GHz is sufficient resolution. We also verified the fast wavelength-switching performance of the ECDL. We triggered the ECDL by a signal from a function generator, and confirmed stable wavelength-switching up to 6.55 kHz. Even when switching wavelengths at high speed, we observed high wavelength reproducibility (< 0.01 nm) and output stability (< 0.39%), which indicates the superiority of the DMD when used as a wavelength selection mechanism. The conventional is-TPG uses a commercial ECDL. It is tuned by actuators, so mechanical motion of its mirror is large and stable high-speed operation is difficult. Computer-driven mirrors, such as galvanometer mirrors, could be used for high-speed wavelength switching. However, in terms of stability and reproducibility, a DMD, which is a MEMS device, has better performance. Thus, we used a DMD for wavelength selection in this work.

Because we obtained the desired characteristics, we used this ECDL as a seed source for the is-TPG and generated THz-waves. First, we measured the frequency tunability of the is-TPG during fast wavelength-switching. We synchronized the ECDL with the pump beam, and detected the detection Stokes beam intensity with a NIR camera when switching among seven wavelengths at 50 Hz. Figure 2(b) shows the tunability of the is-TPG when tuning the THz wavelength in two different ways. The dashed line shows the result of sweeping each wavelength by the conventional method using a commercial ECDL, and the solid line shows the result of fast wavelength-switching; its tunable range was 0.78–2.62 THz, the same as without fast switching.

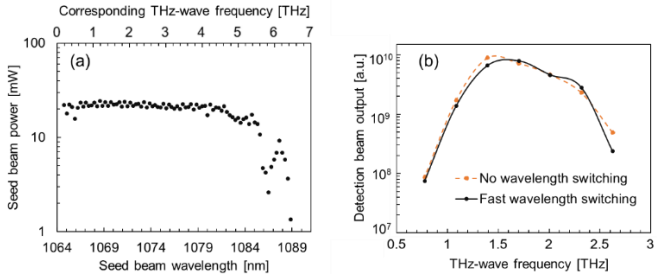

Fig. 2. (a) Tunability of an external cavity diode laser using a digital micromirror device; single-mode oscillation was confirmed. The upper axis shows the corresponding frequency (in THz) when the laser is used as a seed source for an injection-seeded THz-wave parametric generator. (b) Frequency tunability of the generator with (solid black line) and without (dashed orange line) fast wavelength-switching.

Next, we demonstrated switching among 10, and then 17, wavelengths. A "10-wavelength THz-wave" (1.20–1.77 THz) was generated and detected, as shown in Fig. 3(a). We also measured the stability of the detection Stokes beams at each wavelength. The intensity average stability of the 10 wavelengths was 0.95%, which was almost the same as the 0.86% obtained in the case of single wavelength THz-wave generation using the same system. This indicates that fast wavelength-switching does not affect the stability. We show the output in the case with the 17 wavelengths in Fig. 3(b). Due to the exposure time of the NIR camera used, 17 was the maximum number of wavelengths that could be detected in a single frame. Although the detection Stokes beams were not spatially separated by wavelength, we confirmed wavelength-switching for these 17 wavelengths. In addition, Fig. 3(c) shows the results obtained when a reagent (maltose) was inserted into the THz-wave path. Spectral measurement was possible even when the detection Stokes beams were not spatially separated, because the THz-waves were absorbed continuously according to the fingerprint spectrum. The absorption spectra were consistent with those of maltose (Fig. 5[a]), thus confirming that our system is capable of accurate spectral measurements.

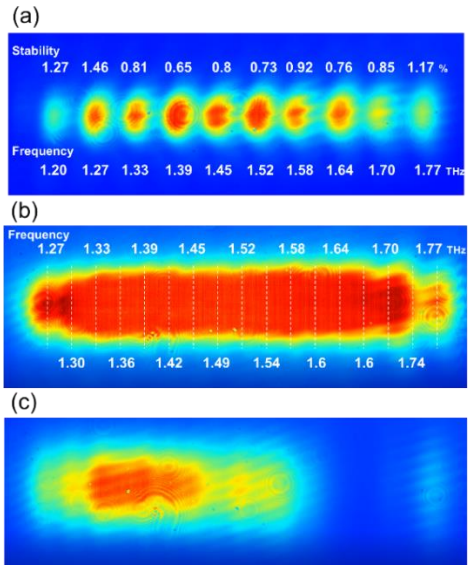

Fig. 3. Detection Stokes beams when (a) switching among 10 wavelengths (1.20–1.77 THz) and (b) switching among 17 wavelengths (1.27–1.77 THz). (c) Maltose was inserted into the THz-wave path while switching among the 17 wavelengths. The interference fringes in Fig. 3(b) and(c) were caused by the coverglass of the CMOS sensor of the NIR camera.

Finally, we demonstrated real-time measurement using the developed system. Because there is a trade-off between the number of THz-wavelengths and the measurement frame rate, we had to use an appropriate number of THz-wavelengths according to the measurement target. In this spectroscopy experiment, we switched among five THz-wavelengths to obtain measurements with the five kinds of reagents. The NIR camera frame rate and exposure time were set to 10 Hz and 100 ms, respectively. Before sample measurement, we evaluated the dynamic range of the system by inserting a calibrated attenuator (three sets of TFA-4; Microtech Instruments, Inc., Eugene, OR, USA) into the THz-wave path and measuring the detection Stokes beam intensity using the NIR camera. As shown in Fig. 4, the detection Stokes beam could be distinguished from the noise until the THz-wave was attenuated to -75 dB. Therefore, the dynamic range of the system was more than 75 dB.

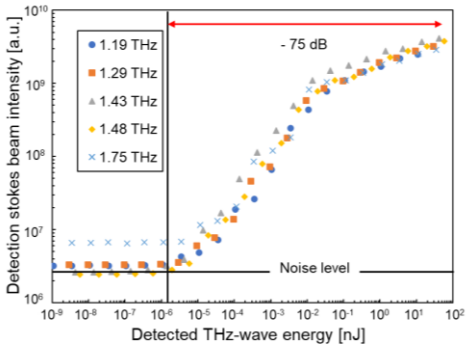

Fig. 4 Input–output characteristics during five-wavelength fast-switching. The dynamic range of this system was 75 dB because the detection Stokes beam could be detected down to an attenuation of 75 dB.

We fine-tuned the wavelengths of this system to match the absorption lines of the reagents, and measured maltose, $Al(OH)_3$, lactose, glucose, and fructose hidden in a cardboard box in real time. The absorption of the five wavelengths of THz-wave changed according to the fingerprint spectra of each reagent, as shown in Fig. 5, and our supplementary file. This result shows that stable real-time measurements were realized by introducing the rapidly wavelength-switchable ECDL using the DMD into the is-TPG.

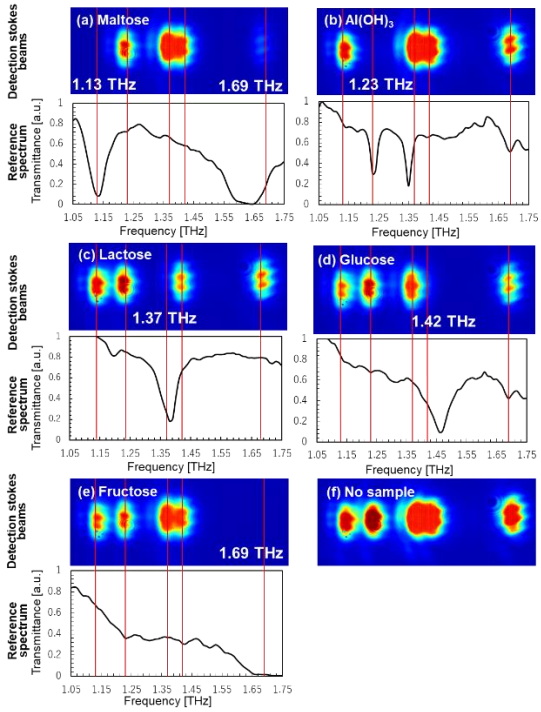

Fig. 5 . Real-time measurement of reagents hidden in a cardboard box. (a–e) Detection Stokes beams with each sample inserted into the path of the THz-waves (upper figures) and the reference spectra of each sample obtained by an injection-seeded THz-wave parametric generator (lower figures). (f) Detection Stokes beams without samples. (see Visualization 1)

In this study, we demonstrated a wide dynamic range, real-time THz measurement system that used a rapidly wavelength-switchable is-TPG. Although the speed of THz-wavelength tuning has previously been limited by the seed source (to almost 1 THz/min), introducing our developed ECDL with a DMD enables wavelength switching that is synchronized with the pump pulse. Moreover, obtaining all THz-wavelength information in one frame is possible by THz parametric detection with a NIR camera. Using this system, sample measurement was realized in real time. In the future, we will aim to increase the pump beam repetition rate to a few hundreds of Hz and explore the practical applications, such as inspection of mail in international post offices.

Funding. This work was partially supported by the Japan Society for the Promotion of Science KAKENHI (18H03887, 19H02627), the Research Foundation for Opto-Science and Technology and The Hibi Science Foundation.

Acknowledgments. The authors appreciate the fruitful discussions with Prof. T. Taira of RIKEN and IMS, Dr. K. Muro and Dr. D. Fukuoka of Spectra Quest Lab, Inc, Dr. S. Hayashi of NICT, and Dr. H. Minamide, Dr. K. Nawata, Dr. Y. Takida of RIKEN.

Disclosures. The authors declare no conflicts of interest.

References

1. Y. Kawada, T. Yasuda, A. Nakanishi, K. Akiyama, and H. Takahashi, Opt. express **19**, 11228–11235 (2011).
2. Y. Nomura, H. Shirai, and T. Fuji, Nat. Commun. **4**, 1–11 (2013).
3. S. M. Teo, B. K. Ofori-Okai, C. A. Werley, and K. A. Nelson, Rev. Sci. Instrum. **86**, 051301 (2015).
4. T. A. Oliver, Royal Soc. **5**, 171425 (2018).
5. C. Hoberg, P. Balzerowski, and M. Havenith, AIP Adv. **9**, 035348 (2019).
6. Q. Wang, L. Xie, and Y. Ying, Appl. Spectrosc. Rev. 1–16 (2021).
7. Y. Wada, T. Satoh, Y. Higashi, and Y. Urata, J Infrared Milli Terahz Waves **38**, 1471–1476 (2017).
8. Y. Moriguchi, Y. Tokizane, Y. Takida, K. Nawata, S. Nagano, M. Sato, T. Otsuji, and H. Minamide, Opt. Lett. **45**, 77–80 (2020).
9. K. B. Cooper, R. J. Dengler, N. Llombart, B. Thomas, G. Chattopadhyay, and P. H. Siegel, IEEE Trans. Terahertz Sci. Technol. **1**, 169–182 (2011).
10. H. Feng, D. An, H. Tu, W. Bu, W. Wang, Y. Zhang, H. Zhang, X. Meng, W. Wei, and B. Gao, Appl. Phys. B **126**, 1–9 (2020).
11. K. Murate, S. Hayashi, and K. Kawase, Appl. Phys. Express **10**, 032401 (2017).
12. R. Mitsuhashi, K. Murate, S. Niijima, T. Horiuchi, and K. Kawase, Opt. Express **28**, 3517–3527 (2020).
13. K. Murate and K. Kawase, J. Appl. Phys **124**, 160901 (2018).
14. S. Hayashi, K. Nawata, T. Taira, J. Shikata, K. Kawase, and H. Minamide, Sci. Rep. **4**, 1–5 (2014).
15. K. Murate, H. Sakai, and K. Kawase, IEEE Trans. Terahertz Sci. Technol. **10**, 200–203 (2020).
16. H. Sakai, K. Kawase, and K. Murate, Opt. Lett. **45**, 3905–3908 (2020).
17. M. Kato, S. R. Tripathi, K. Murate, K. Imayama, and K. Kawase, Opt. express **24**, 6425–6432 (2016).
18. M. A. Gutin and J. Castracane, in *Testing, Packaging, Reliability, and Applications of Semiconductor Lasers IV* **3626**, 53–60 (1999).
19. N. Riza and M. J. Mughal, Opt. Express **11**, 1559 (2003).
20. M. Breede, C. Kasseck, C. Brenner, N. C. Gerhardt, M. Hofmann, and R. Hofling, Electron. Lett. **43**, 456–457 (2007).
21. F. Havermeyer, L. Ho, and C. Moser, Opt. Express **19**, 14642–14652 (2011).
22. J. Li, X. Chen, M. Lv, Y. Gao, and G. Chen, Appl. Phys. B **125**, 30 (2019).
23. S. Mine, K. Kawase, and K. Murate, Appl. Opt. **60**, 1953–1957 (2021).

Full References

1. Y. Kawada, T. Yasuda, A. Nakanishi, K. Akiyama, and H. Takahashi, "Single-shot terahertz spectroscopy using pulse-front tilting of an ultra-short probe pulse," Optics express **19**, 11228–11235 (2011).
2. Y. Nomura, H. Shirai, and T. Fuji, "Frequency-resolved optical gating capable of carrier-envelope phase determination," Nature Communications **4**, 1–11 (2013).
3. S. M. Teo, B. K. Ofori-Okai, C. A. Werley, and K. A. Nelson, "Invited Article: Single-shot THz detection techniques optimized for multidimensional THz spectroscopy," Review of Scientific Instruments **86**, 051301 (2015).
4. T. A. Oliver, "Recent advances in multidimensional ultrafast spectroscopy," Royal Society open science **5**, 171425 (2018).
5. C. Hoberg, P. Balzerowski, and M. Havenith, "Integration of a rapid scanning technique into THz time-domain spectrometers for nonlinear THz spectroscopy measurements," AIP advances **9**, 035348 (2019)
6. Q. Wang, L. Xie, and Y. Ying, "Overview of imaging methods based on terahertz time-domain spectroscopy," Applied Spectroscopy Reviews 1–16 (2021).
7. Y. Wada, T. Satoh, Y. Higashi, and Y. Urata, "Compact Tunable Narrowband Terahertz-Wave Source Based on Difference Frequency Generation Pumped by Dual Fiber Lasers in MgO:$LiNbO_3$," J Infrared Milli Terahz Waves **38**, 1471–1476 (2017).
8. Y. Moriguchi, Y. Tokizane, Y. Takida, K. Nawata, S. Nagano, M. Sato, T. Otsuji, and H. Minamide, "Frequency-agile injection-seeded terahertz-wave parametric generation," Optics Letters **45**, 77–80 (2020).
9. K. B. Cooper, R. J. Dengler, N. Llombart, B. Thomas, G. Chattopadhyay, and P. H. Siegel, "THz imaging radar for standoff personnel screening," IEEE Transactions on Terahertz Science and Technology **1**, 169–182 (2011).
10. H. Feng, D. An, H. Tu, W. Bu, W. Wang, Y. Zhang, H. Zhang, X. Meng, W. Wei, and B. Gao, "A passive video-rate terahertz human body imager with real-time calibration for security applications," Applied Physics B **126**, 1–9 (2020).
11. K. Murate, S. Hayashi, and K. Kawase, "Multiwavelength terahertz-wave parametric generator for one-pulse spectroscopy," Applied Physics Express **10**, 032401 (2017).
12. R. Mitsuhashi, K. Murate, S. Niijima, T. Horiuchi, and K. Kawase, "Terahertz tag identifiable through shielding materials using machine learning," Optics Express **28**, 3517–3527 (2020).
13. K. Murate and K. Kawase, "Perspective: Terahertz wave parametric generator and its applications," J. Appl. Phys **124**, 160901 (2018).
14. S. Hayashi, K. Nawata, T. Taira, J. Shikata, K. Kawase, and H. Minamide, "Ultrabright continuously tunable terahertz-wave generation at room temperature," Scientific Reports **4**, 1–5 (2014).
15. K. Murate, H. Sakai, and K. Kawase, "Six-Billion-Fold Amplification via a Two-Stage Terahertz Parametric Amplifier," IEEE Transactions on Terahertz Science and Technology **10**, 200–203 (2020).
16. H. Sakai, K. Kawase, and K. Murate, "Highly sensitive multi-stage terahertz parametric detector," Optics Letters **45**, 3905–3908 (2020).
17. M. Kato, S. R. Tripathi, K. Murate, K. Imayama, and K. Kawase, "Non-destructive drug inspection in covering materials using a terahertz spectral imaging system with injection-seeded terahertz parametric generation and detection," Optics express **24**, 6425–6432 (2016).
18. M. A. Gutin and J. Castracane, "Fast tunable diode laser with digital control and multiple line selection," in *Testing, Packaging, Reliability, and Applications of Semiconductor Lasers IV* **3626**, 53–60 (1999).
19. N. Riza and M. J. Mughal, "Broadband optical equalizer using fault tolerant digital micromirrors," Optics Express **11**, 1559 (2003).
20. M. Breede, C. Kasseck, C. Brenner, N. C. Gerhardt, M. Hofmann, and R. Hofling, "Micromirror device controlled tunable diode laser diode laser," Electronics Letters **43**, 456–457 (2007).
21. F. Havermeyer, L. Ho, and C. Moser, "Compact single mode tunable laser using a digital micromirror device," Optics Express **19**, 14642–14652 (2011).
22. J. Li, X. Chen, M. Lv, Y. Gao, and G. Chen, "16-Port tunable fiber laser based on a digital micromirror device in C-band," Applied Physics B **125**, 30 (2019).
23. S. Mine, K. Kawase, and K. Murate, "High-power ASE-free fast wavelength-switchable external cavity diode laser," Applied Optics, **60**, 1953–1957 (2021).